Petroleum Science 22 (2025) 2592–2603

Contents lists available at ScienceDirect

Petroleum Science

journal homepage: www.keaipublishing.com/en/journals/petroleum-science

Original Paper

Origins of steam-mediated selectivity improvement in the oxidative coupling of methane over MnO_x-Na_2WO_4/SiC

Juan Chen [a, b, 1], Jian-Shu Li [a, b, 1], Anna Zanina [b], Wen Jiang [a], Yu-Ming Li [a], Gui-Yuan Jiang [a, *], Evgenii V. Kondratenko [b, **]

[a] State Key Laboratory of Heavy Oil Processing, China University of Petroleum Beijing, Beijing, 102249, China
[b] Leibniz Institut für Katalyse e.V., Albert-Einstein-Str. 29a, 18059, Rostock, Germany

ARTICLE INFO

Article history:
Received 11 December 2024
Received in revised form
27 April 2025
Accepted 6 May 2025
Available online 7 May 2025

Edited by Min Li

Keywords:
Oxidative coupling of methane
Active oxygen species
5NaW-3Mn/SiC
Steam effect

ABSTRACT

Oxidative coupling of methane (OCM) is one of the most promising approaches to produce ethylene and ethane (C_2-hydrocarbons) in the post-oil era. The MnO_x-Na_2WO_4/SiO_2 system shows promising OCM performance, which can be further enhanced by cofed steam. However, the positive effect of steam on C_2-hydrocarbons selectivity practically disappears above 800 °C. In the present study, we demonstrate that the use of SiC as a support for MnO_x-Na_2WO_4 is beneficial for achieving high selectivity up to 850 °C. Our sophisticated kinetic tests using feeds without and with steam revealed that the steam-mediated improvement in selectivity to C_2-hydrocarbons is due to the inhibition of the direct CH_4 oxidation to carbon oxides because of the different enhancing effects of steam on the rates of CH_4 conversion to C_2H_6 and CO/CO_2. Other descriptors of the selectivity improvement are MnO_x dispersion and the catalyst specific surface area. The knowledge gained herein may be useful for optimizing OCM performance through catalyst design and reactor operation.

1. Introduction

Natural gas is abundant in reserves and widely distributed and is composed of 70%–90% methane (Holmen, 2009; Schwach et al., 2017; Wang et al., 2022). Its efficient utilization will greatly alleviate the global energy crisis and reduce the dependence on oil resources (Kondratenko et al., 2017). Among various reaction routes, the oxidative coupling of methane (OCM) has attracted much attention due to its advantage to produce C_2H_6 and C_2H_4 (C_2-hydrocarbons) from CH_4 in an eco-friendly and energy efficient manner (Liu et al., 2022; Xu et al., 2022).

As a typical highly exothermic reaction, OCM is not thermodynamically limited (Matsumoto et al., 2020; Sourav et al., 2021). The yield of C_2-hydrocarbons achieved up to now is, however, lower than 30%, which hinders any commercialization of the OCM reaction to some extent. The activation of C–H bonds in the feed alkane is the main bottleneck of the OCM reaction (Li X. et al., 2020; Tang et al., 2014; Wang et al., 2021). In addition, the desired C_2-hydrocarbons are more reactive than methane and therefore they are easily oxidized to carbon oxides, which reduces their yield. Since the discovery of the OCM reaction in 1980s by Keller and Bhasin (1982), multiple efforts have been made to increase the selectivity to C_2-hydrocarbons. The NaWMn/SiO_2 system (Fang et al. 1992a, 1992b; Li, 2001) is generally accepted to be promising in view of high C_2-hydrocarbons selectivity and on-stream stability. Although this system has been thoroughly investigated, the knowledge about factors affecting the formation of selective and side products is still limited. For example, a recent study indicates that W and Mn species can stabilize the catalyst and catalyze oxygen during the OCM reaction, respectively (Werny et al., 2020). Some previous studies highlighted the importance of the Mn^{2+} and Mn^{3+} redox cycle in O_2 activated during the OCM reaction (Fleischer et al., 2018; Li, 2001). Sinev et al. investigated the redox behavior of MnO_x-Na_2WO_4/SiO_2 catalyst, indicating that the crystalline Na_2WO_4 and Mn_2O_3 phases disappeared during the oxygen desorption process, forming crystalline $MnWO_4$ and colloidal substances (possibly amorphous Na_2MnO_2) (Sinev et al., 2019).

The NaWMn/SiO_2 system is also characterized by a positive effect

* Corresponding author.
** Corresponding author.
E-mail addresses: jianggy@cup.edu.cn (G.-Y. Jiang), Evgenii.Kondratenko@catalysis.de (E.V. Kondratenko).
[1] These authors contributed equally.

https://doi.org/10.1016/j.petsci.2025.05.001

of cofed steam on the selectivity to C_2-hydrocarbons and overall catalyst activity (Alzahrani and Lobban, 1995; Aydin et al., 2020; Aydin et al. 2021; Aydin et al. 2022; Chin et al., 2011; Dooley et al., 1994; Li D. et al., 2020; Li et al., 2021; Li J. et al., 2023; Li et al., 1996; Liang et al., 2014; Lomonosov et al., 2013; Pereira et al., 1990; Shimizu et al., 2001; Takanabe and Iglesia, 2008, 2009; Xu et al., 2023; Zanina et al., 2022, 2023, 2024). Takanabe and Iglesia (2008) suggested that steam could enhance the selectivity due to the formation of OH radicals. An alternative explanation was provided by Lomonosov et al. (2013), steam accelerates the regeneration of surface oxygen species. Our group has suggested that steam contributes to the conversion of adsorbed diatomic oxygen species into monoatomic ones, which is favorable for hindering the direct CH_4 oxidation to CO_2 (Aydin et al., 2020). The strength of the positive effect of steam was found to depend on the kind of support for the NaWMn active component (Zanina et al., 2024).

To the best of our knowledge, the effect of steam on the OCM reaction over SiC-supported NaWMn-based catalysts have not been investigated. SiC, because of its remarkable thermal conductivity (100–200 $W \cdot m^{-1} \cdot K^{-1}$), outstanding mechanical strength, excellent stability at high temperature and chemical inertness, has been used for heterogeneous catalysts as a support (Ercolino et al., 2017; Le et al., 2018; Liao et al., 2019; Wang et al., 2017). Liu and co-authors used SiC monolithic foam as a support to improve thermal properties of catalysts for the OCM reaction (Liu et al., 2008) through inhibiting rapid temperature rise. SiC support can also be attractive due to its high-temperature electronic properties. In condensed matter physics, when two or more two-dimensional materials are stacked together with a certain lattice mismatch or torsion angle, the surface may form a large period of moiré fringes. This superstructure with long-range quasi-periodic patterns is called moiré superlattice (Liu et al., 2021; Novoselov et al. 2004, 2005). In the past decade, two-dimensional materials such as graphene and transition metal dichalcogenides have flourished as atomic-level Lego building blocks. Artificial moiré superlattices, formed by stacking 2D materials with twist angles and/or lattice

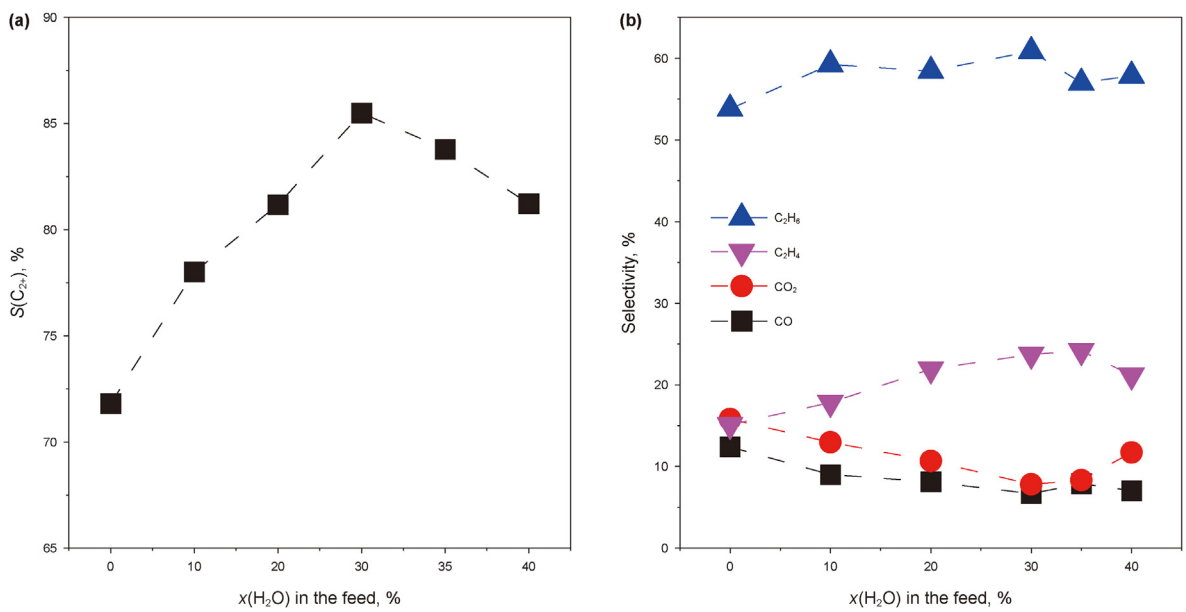

Fig. 1. The effect of steam content on selectivity to **(a)** C_{2+}-hydrocarbons, **(b)** CO, CO_2, C_2H_6 and C_2H_4 over the 5NaW-3Mn/SiC catalyst at 800 °C. Catalyst was varied between 35 and 190 mg to achieve a methane conversion of about 4.5%.

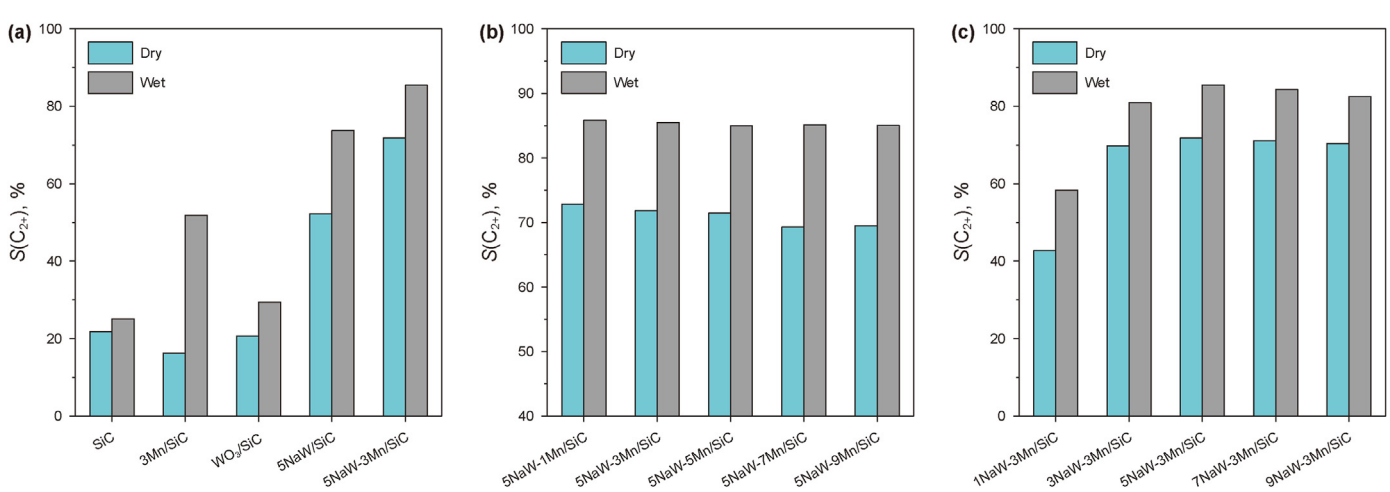

Fig. 2. The selectivity to C_{2+}-hydrocarbons over **(a)** SiC, 3Mn/SiC, WO_3/SiC, 5NaW/SiC, 5NaW-3Mn/SiC, **(b)** 5NaW-*m*Mn/SiC (the content of Na_2WO_4 is 5 wt%, $m = 1, 3, 5, 7, 9$ wt%), **(c)** *m*5NaW-3Mn/SiC (the content of Mn is 3 wt%, $m = 1, 3, 5, 7, 9$ wt%) without (blue) and with 30 vol% (gray) steam. $X(CH_4) = 4.5\%$, $m_{cat} = 13–1680$ mg.

mismatches, have recently become a fertile playing field, exhibiting a host of emergent properties beyond their building blocks. These rich quantum phenomena originate from its non-trivial electronic structure and are effectively regulated by the moiré period (He et al., 2021; Li Y. et al., 2023). The twisted graphene systems from a large twist angle of 30° resulting in a quasicrystal (30°-TBG) to a small "magic" twist angle near 1.1° realizing strongly correlated physics. The scope is then expanded from bilayer to trilayer systems. 30°-TBG is a two-dimensional quasicrystal with twelve-fold rotational symmetry but lacking long-range periodicity, which has been successfully performed on Pt (111), SiC, and Cu (111) (Ahn et al., 2018; Bostwick et al., 2007; Deng et al., 2020; Weng et al., 1998; Yan et al., 2019; Yao et al., 2018). The special construction can improve the transformation of electron thus it can help the catalysts produce more selective oxygen species.

In view of the above discussion, the aim of the present study was to extend the knowledge of the fundamentals related to the improvement of the selectivity to C_2-hydrocarbons over catalysts based on the NaWMn active component. In particular, we decided to investigate if and how the use of SiC as a support for this component is crucial for the positive effect of cofed steam on the OCM performance. To this end, a series of mono-, bi-, and tri-metallic SiC-supported catalysts have been prepared and tested for the activity and product selectivity in the absence and the presence of cofed steam. Selectivity-conversion relationships were determined to check whether and how product selectivity is affected by steam. The results of catalytic tests have been complemented by sophisticated catalyst characterization studies using X-ray diffraction, scanning transmission electron microscopy (STEM), X-ray absorption spectroscopy (XAS), X-ray photoelectron spectroscopy (XPS) and temperature-programmed catalyst reduction with H_2 (H_2-TPR).

2. Materials and methods

2.1. Experimental section

Catalyst synthesis. All chemicals used for catalyst preparation were of analytical purity and not further purification. The 5NaW-3Mn/SiC (5 wt% Na_2WO_4 and 3 wt% Mn) catalyst was synthesized according to a previous report (Pak et al., 1998), by a two-step incipient-wetness impregnation method. First, an aqueous solution of $Mn(NO_3)_2 \cdot 4H_2O$ (Merck, 98.5%) was added to SiC (Macklin, 0.5–0.7 μm, 99%) under stirring. The resulting slurry was putted in an oven at 130 °C for 5 h. The obtained solid material was impregnated with an aqueous solution of $Na_2WO_4 \cdot 2H_2O$ (Sigma Aldrich, 99%) and dried in an oven at 130 °C for 5 h followed by heating to 800 °C with a heating rate of 10 °C·min^{-1}. The catalyst precursor was calcined at 800 °C for 8 h. In one series of catalysts, the amount of MnO_x was 1, 5, 7 or 9 wt% and the mass of Na_2WO_4 was fixed to 5 wt%. The resulting catalysts are named as 5NaW-1Mn/SiC, 5NaW-5Mn/SiC, NaW-7Mn/SiC, 5NaW-9Mn/SiC. In another series of catalysts, the amount of Na_2WO_4 was 1, 3, 7 or 9 wt% and the amount of MnO_x was set to 3 wt%. These catalysts are named as 1NaW-3Mn/SiC, 3NaW-3Mn/SiC, 5NaW-3Mn/SiC, 7NaW-3Mn/SiC, 9NaW-3Mn/SiC. The 5NaW/SiC and 3Mn/SiC catalysts were impregnated only with an aqueous solution of Na_2WO_4 and $Mn(NO_3)_2 \cdot 4H_2O$, respectively. All the catalysts were pressed into pellets, crushed and sieved to 40–60 mesh before catalytic tests.

2.2. Catalyst characterization

X-ray diffraction patterns (XRD) were collected using a BRUKER D8 ADVANCE X-ray powder diffractometer with Cu-Kα (λ = 0.15406 nm) radiation and a Nickel filter operating at 40 kV and 10 mA. The 2θ range was from 15° to 90° at a scanning rate of 4°·min^{-1}.

High-resolution transmission electron microscopy (HRTEM) tests were performed on a FEI F20 electron microscope equipped with a field emission source. Images were recorded with a high angle annular dark field (HAADF) detector.

Temperature-programmed reduction tests with hydrogen (H_2-TPR) were carried out to investigate the reducibility of fresh and spent catalysts. 100 mg of each catalyst were placed into a continuous-flow fixed-bed quartz reactor. The reactor was initially heated in air with a heating rate of 10 °C·min^{-1} to 800 °C and tempered for 1 h followed by cooling in air to room temperature. Next, the reactor was purged with argon (10 mL·min^{-1}) for 30 min. After that, the catalyst was heated up to 900 °C with a temperature rate of 10 °C·min^{-1} and in a flow of 5 vol% hydrogen in argon (10 mL·min^{-1}). The hydrogen and argon were detected by a connected online mass spectrometer (Pfeiffer Vacuum Omnistar GSD320 03).

X-ray photoelectron spectroscopy (XPS) experiments were performed on a Thermo Fisher K-Alpha instrument. The C 1s peak at 284.6 eV was used to calibrate the binding energies.

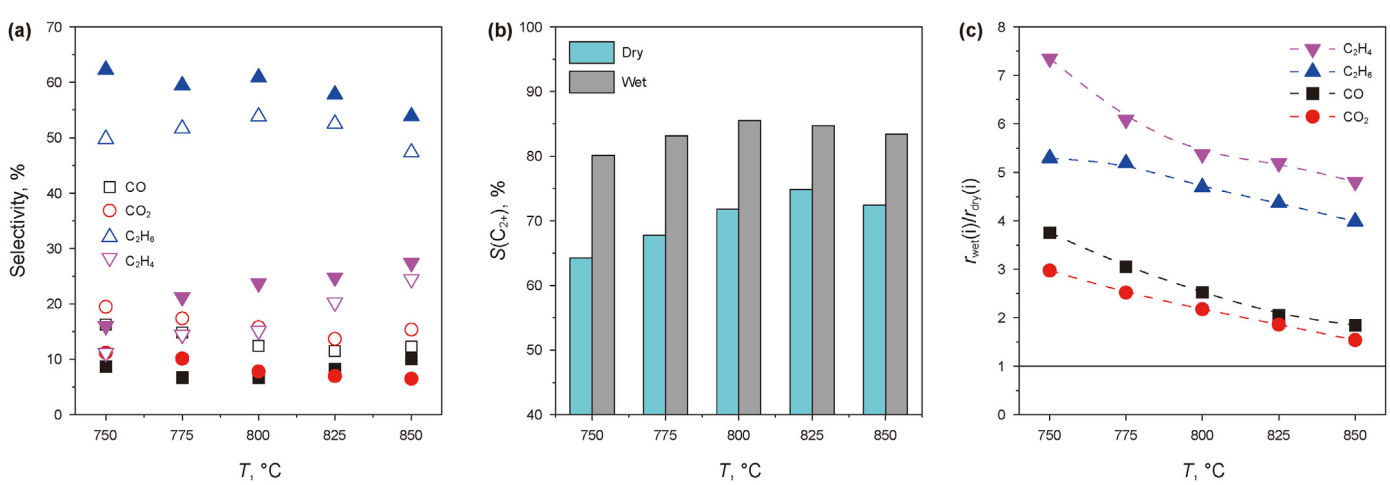

Fig. 3. **(a)** Selectivity to C_2H_6, C_2H_4, CO and CO_2, and **(b)** selectivity to C_{2+}-hydrocarbons with (filled symbols) and without steam (empty symbols), **(c)** the ratio of the CH_4 conversion rate into C_2H_4 (magenta), C_2H_6 (blue), CO (black) and CO_2 (red) with 30 vol% and without steam over 5NaW-3Mn/SiC at different temperature. $X(CH_4)$ = 4.5%, m_{cat} = 20–630 mg.

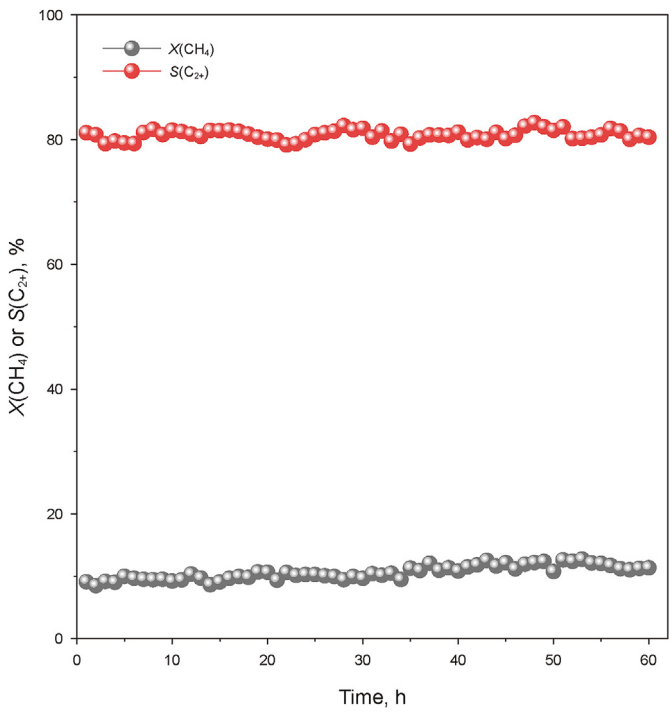

Fig. 4. CH_4 conversion and C_{2+}-hydrocarbons selectivity in a 60 h test using 5NaW-3Mn/SiC with co-fed steam. Reaction conditions: $CH_4/O_2/H_2O/Ar$ = 40/5/30/25, T = 800 °C, F = 30 mL·min^{-1}, τ = 1.67 gg·min·L^{-1}.

Nitrogen adsorption-desorption isotherms (BET) were recorded using a Micromeritics ASAP 2460 instrument. The samples were pretreated at 90 °C for 1 h and then at 300 °C for 4 h in vacuum.

The elemental content of each catalyst was determined by inductively coupled plasma optical emission spectrometry (ICP-OES) on a Thermo Fisher IRIS Intrepid II.

The XANES spectra (Mn K-edge) were measured at the BL11B station on the Shanghai Synchrotron Radiation Facility. The samples were deposited on double-sided carbon tape using a Lytle detector. Mn foil and MnO_2 were used as references and measured in a transmission mode using an ionization chamber.

2.3. Catalytic tests

OCM performance was determined under continuous flow conditions in a fixed bed quartz micro reactor. A certain amount of catalyst was fixed in the reactor by quartz wool. The reactor was heated in air to 800 °C with a heating rate of 10 °C·min^{-1}. The OCM tests without or with cofed steam (30 vol%) were performed using a feed with 40 vol% CH_4 (99.999%) and CH_4/O_2 (99.999%) molar ratio of 8:1. Argon (99.99%) was used as inert standard. The total feed flow was 30 mL·min^{-1}.

The main outlet gas-phase components were CO, CO_2, H_2O, O_2, Ar, CH_4, C_2H_6, C_2H_4, C_3H_8 and C_3H_6. The concentration of the feed components and the reaction products was determined by an on-line gas chromatograph SP-3420A equipped with a thermal conductivity detector (Porapak Q and TDX-01 columns), in order to separate Ar, O_2, CO and CO_2. A flame ionization detector was connected to a GS-Alumina column used to separate CH_4, C_2H_6, C_2H_4, C_3H_8 and C_3H_6. Methane and oxygen conversion ($X(A)$), product selectivity ($S(i)$), the rate of methane conversion ($r(CH_4)$) and the rate of methane conversion into products ($r(i)$) were calculated using Eqs. (1)–(4), respectively. The selectivity to C_2H_6, C_2H_4, C_3H_8 and C_3H_6 was abbreviated as $S(C_{2+})$.

$$X(A) = \left(1 - \frac{x_A^{in}}{x_A^{out}}\right) \times 100\% \quad (1)$$

$$S(i)\% = \frac{v_i}{v_{CH_4}} \times \frac{x_i^{out}}{x_{CH_4}^{in} - x_{CH_4}^{out}} \times 100\% \quad (2)$$

$$r(CH_4) = \frac{x_{CH_4}^0 \times F_{feed}}{m_{cat} \times V_m} \times \left(X(CH_4) - X^0(CH_4)\right) \quad (3)$$

$$r(i) = S(i) \times r(CH_4) \quad (4)$$

where, x is the mole fraction. $X^0(CH_4)$ denotes methane conversion when there is absence of catalyst, and that corresponds to the y-intercept. The carbon balance determined for all catalysts was found to be about 96%–99%.

3. Results and discussion

3.1. Catalyst activity and product selectivity with and without cofed steam

In agreement with previous studies using $NaWMn/SiO_2$ catalysts (Aydin et al., 2020, 2021, 2022), the selectivity to C_{2+}-hydrocarbons at a methane conversion of about 4.5% over the 5NaW-3Mn/SiC catalyst in the present study was also improved by co-fed steam (Fig. 1(a)). The highest selectivity of 85.5% was achieved using the feed with 30 vol% steam. The selectivity decreased with a further increase in steam content. The steam-mediated increase in the selectivity to C_{2+}-hydrocarbons was mainly caused by a decrease in CO_2 production and, to a lesser extent, in CO production (Fig. 1(b)). This result is consistent with our previous work using $NaWMn/SiO_2$ catalysts (Aydin et al., 2020, 2021; Li et al., 2023; Zanina et al., 2022).

To analyze the role of individual components of the NaW-Mn/SiC system in the increasing steam effect, bare support and monocomponent catalysts were prepared and tested (Fig. 2(a)). For all catalysts, the selectivity to C_{2+}-hydrocarbons was improved by steam, with the highest increase being determined for the 3Mn/SiC catalyst. Nevertheless, the latter catalyst is less selective as compared to the 5NaW/SiC catalyst, which shows, however, lower C_{2+}-hydrocarbons selectivity than the 5NaW-3Mn/SiC catalyst. Thus, the presence of all individual catalyst components is needed to achieve the highest selectivity through co-fed steam, although the increase in the selectivity is the least pronounced (Fig. 2(a)).

The positive steam effect was also found for other catalysts differing in the ratio of MnO_x to Na_2WO_4. The selectivity to C_{2+}-hydrocarbons slightly decreases with increasing MnO_x content at a fixed Na_2WO_4 loading of 5 wt% in OCM tests without co-fed steam and hardly changes in the presence of this feed component (Fig. 2(b)). Regardless of the feed content of steam, the selectivity of catalysts with a fixed MnO_x loading increases with increasing Na_2WO_4 content (Fig. 2(c)). When the content of the latter component is higher than 3 wt%, no selectivity improvements could be found.

Using a feed with 30 vol% steam, we also investigated how this feed component influences product selectivity over the 5NaW-3Mn/SiC catalyst in the temperature range between 750 and 850 °C (Fig. 3(a) and (b)). In the absence of steam, the selectivity to C_{2+}-hydrocarbons at about 4.5% CH_4 conversion increased with an increase in the temperature from 750 to 825 °C, and slightly decreased when the temperature was further increased to 850 °C. In the presence of steam, the selectivity was improved at all temperatures

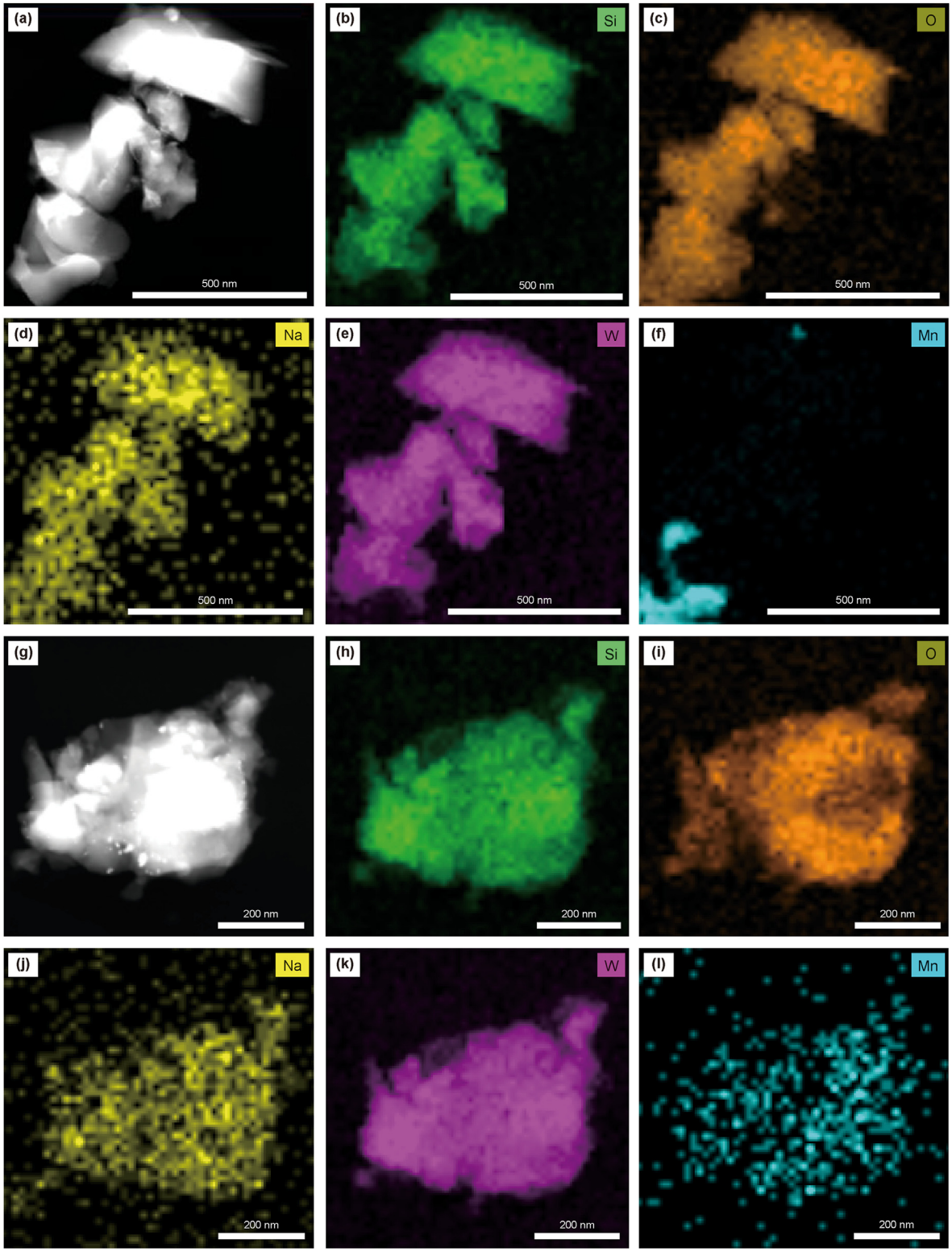

Fig. 5. STEM images and EDX images of Si (green), O (orange), Na (yellow), W (amaranth) and Mn (cyan) elements over 5NaW-3Mn/SiC fresh (**(a)**–**(f)**) and spent with steam (**(g)**–**(l)**).

but passed a maximum of 85.5% at 800 °C. This improvement is due to a decrease in selectivity to CO and CO_2 (Fig. 3(a)). The negative effect on the selectivity to CO passed a maximum at about 800 °C, while the strength of the steam mediated decrease in the selectivity to CO_2 decreased with increasing temperature. Consequently, the improvement in C_{2+}-hydrocarbons selectivity also decreased.

The kinetic origins of the steam effects described above were elucidated by analyzing the rates of methane conversion to individual reaction products. To this end, we plotted the ratio of each rate determined in the presence of steam to that in the absence of

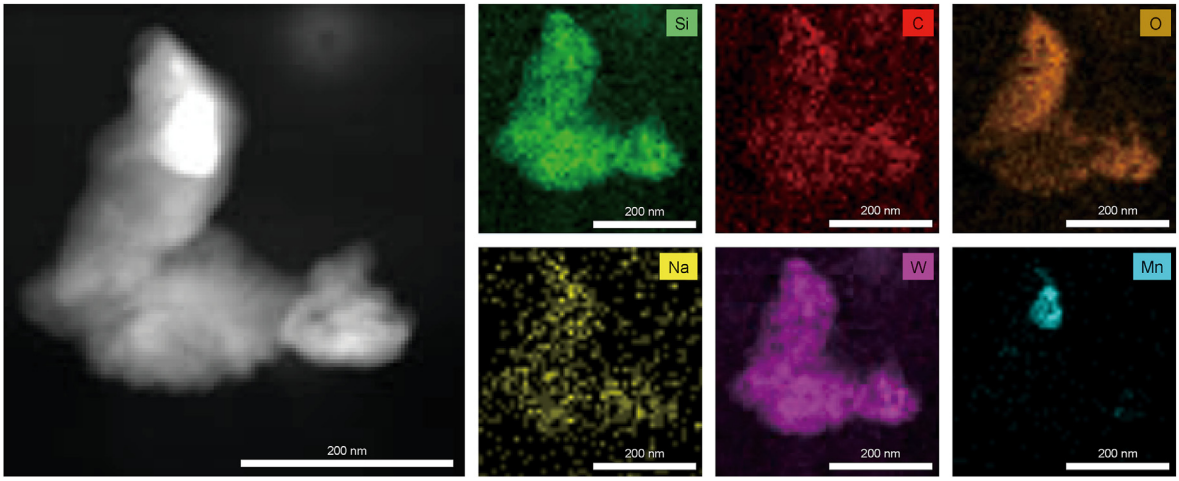

Fig. 6. STEM images and EDX images of spent 5NaW-3Mn/SiC without steam.

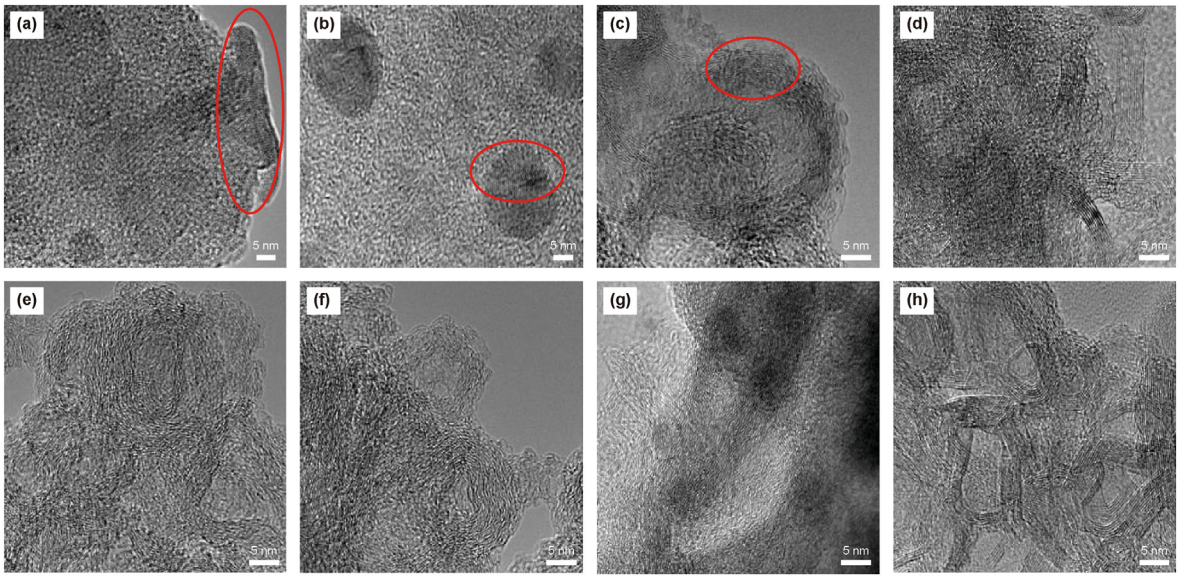

Fig. 7. TEM images of fresh ((**a**), (**b**)) 1NaW-3Mn/SiC, ((**c**), (**d**)) 3NaW-3Mn/SiC, ((**e**), (**f**)) 5NaW-3Mn/SiC and ((**g**), (**h**)) 7NaW-3Mn/SiC.

Table 1
BET surface area, pore volume and pore diameter of fresh and spent SiC, 3Mn/SiC, 5NaW/SiC and 5NaW-3Mn/SiC with and without steam.

Sample	S_{BET}, $m^2 \cdot g^{-1}$	V_{abs}, $cm^3 \cdot g^{-1}$	D_{abs}, nm
SiC	18	0.07	23.6
3Mn/SiC	18	0.08	22.3
5NaW/SiC	5	0.06	8.30
5NaW-3Mn/SiC	6	0.01	6.60
SiC dry	17	0.08	31.1
3Mn/SiC dry	13	0.06	25.5
5NaW/SiC dry	4	0.00	3.0
5NaW-3Mn/SiC dry	7	0.01	4.40
SiC wet	13	0.07	58.8
3Mn/SiC wet	14	0.06	26.0
5NaW/SiC wet	2	/	/
5NaW-3Mn/SiC wet	3	/	/

V_{abs} is mainly BJH adsorption cumulative volume of pores.
D_{abs} is mainly BJH adsorption average pore diameter.

steam (r_{wet}/r_{dry}) versus the reaction temperature (Fig. 3(c)). For all products, this ratio is above 1, i.e., steam accelerates all rates but to a different extent. The highest increase was achieved for the formation of C_2H_4, followed by C_2H_6, CO and CO_2. It is worth mentioning that this improvement order differs from that determined previously for the NaW-Mn/SiO_2 system, for which the highest increase was determined for the rate of CO formation (Aydin et al., 2020). For all products formed over the 5NaW-3Mn/SiC catalyst in the present study, the strength of the acceleration of their formation rates decreases with increasing temperature. The strongest decrease by about factor of 2 was determined for the rates of CH_4 conversion to CO and CO_2. The ratio of r_{wet}/r_{dry} for CO, CO_2, C_2H_6 and C_2H_4 at 850 °C is 1.8, 1.5, 4.0 and 4.8, respectively. The value for CO is significantly lower as compared to that previously determined for the NaW-Mn/SiO_2 (Aydin et al., 2020), while the values for C_2H_6 and C_2H_4 are similar.

In the OCM reaction, the catalysts should show not only excellent methane conversion and selectivity to C_{2+}-hydrocarbons, but

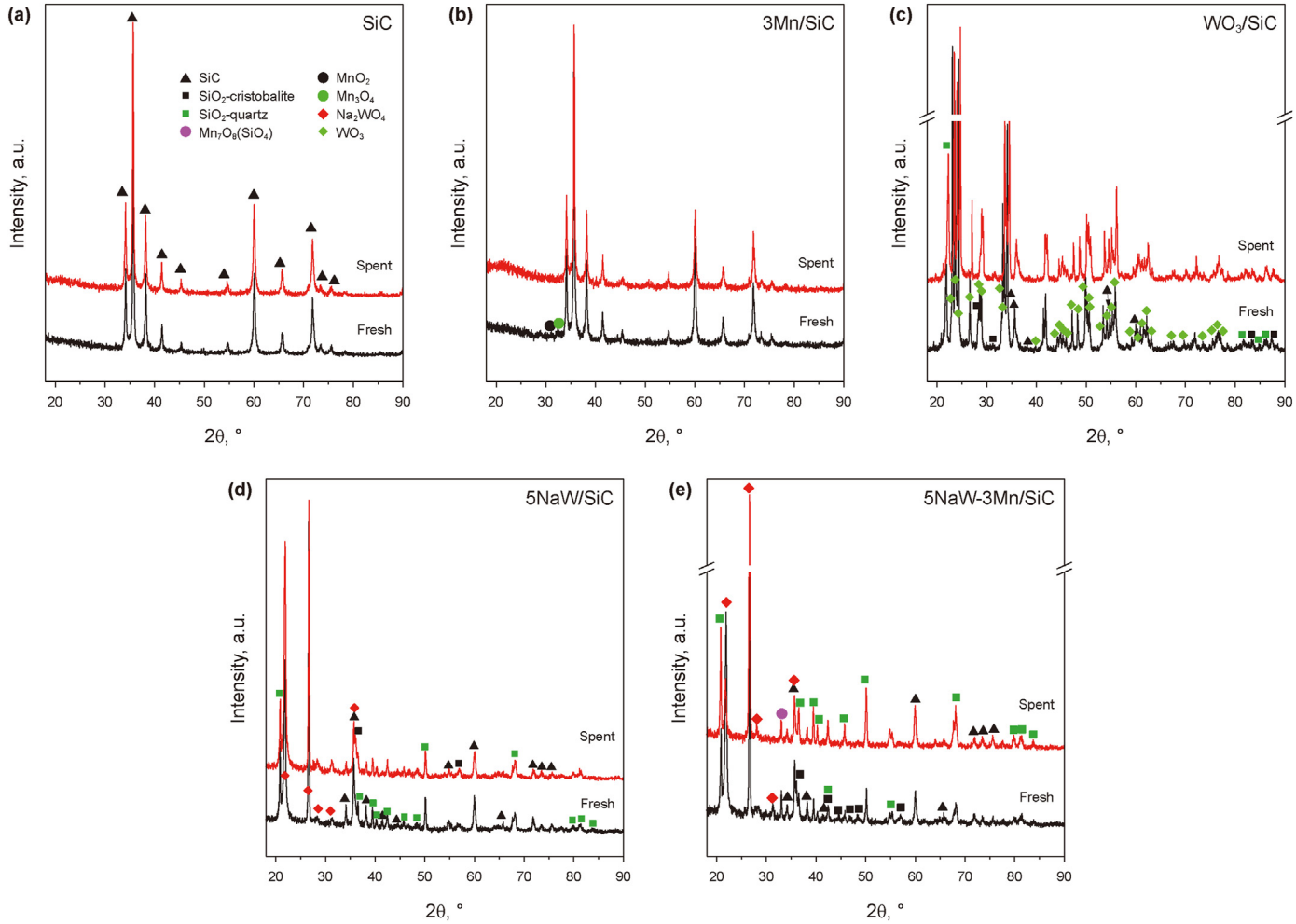

Fig. 8. XRD patterns of **(a)** SiC, **(b)** 3Mn/SiC, **(c)** WO_3/SiC, **(d)** 5NaW/SiC and **(e)** 5NaW-3Mn/SiC fresh and spent with steam.

also high on-stream stability. For this purpose, we tested 5NaW-3Mn/SiC for 60 h. The results obtained are shown in Fig. 4. The CH_4 conversion increased slightly with increasing time and the selectivity to C_{2+}-hydrocarbons showed no obvious changes. It illustrates the excellent on-stream stability of the catalyst.

3.2. Physical properties of catalysts

The distribution of Si, Na, W, O and Mn on the surface of fresh and spent 5NaW-3Mn/SiC catalyst samples used in the OCM reaction without or with co-fed steam was investigated by scanning transmission electron microscopy (STEM) with EDX (Figs. 5 and 6). No obvious difference between the different samples in the distribution of Si, Na, W, O could be found. However, the dispersion of Mn-containing species increased after the OCM reaction with co-fed steam in agreement with a previous study using a similar SiO_2-supported catalyst (Aydin et al., 2020). This can be a reason of the positive effect of steam on the selectivity to C_{2+}-hydrocarbons over 3Mn/SiC and 5NaW-3Mn/SiC (Fig. 2(a) and (c)).

HRTEM images of fresh *m*NaW-3Mn/SiC (m = 1%, 3%, 5%, 7%) catalysts are shown in Fig. 7. Moiré superlattices (red dotted frame) are seen in the images of all catalysts and they become more evident when the amount of Na_2WO_4 in the catalysts increases (Abbas et al., 2020). As typical semiconductors, SiC, MnO_x and Na_2WO_4 react with each other and the heterojunctions interface leads to the modifications of the electronic structure resulting in such superlattices (Abbas et al., 2020), which is in favor of improving selectivity to C_{2+}-hydrocarbons. The structure of moiré superlattices can also generate more electrons and holes and separate them quickly, optimizing the electronic property of catalysts under high temperature to improve the selectivity to C_{2+}-hydrocarbons.

The BET surface area and pore diameter of SiC, 5NaW/SiC and 5NaW-3Mn/SiC decreased after impregnating with Na_2WO_4 (Table 1). This finding suggests that the Na_2WO_4 is loaded on the surface of SiC. The BET surface area decreased further after the catalysts have been used in OCM with co-fed steam. This decrease of surface area is consistent with STEM data for the redispersion effect of steam on MnO_x.

Fresh and spent SiC, 3Mn/SiC, 5NaW/SiC, WO_3/SiC and 5NaW-3Mn/SiC catalysts were also characterized by ex situ XRD (Fig. 8). The XRD patterns of all SiC samples have reflections typical for the hexagonal SiC structure (JCPDS No.01-074-1302) (Xu et al., 2021). After depositing MnO_x on the surface of SiC, two additional weak diffraction peaks centered at 28.7° and 32.4° appeared. They belong to MnO_2 (JCPDS No.00-050-0866) and Mn_3O_4 (JCPDS No.01-075-1560), respectively (Lolupiman et al., 2019; Yang et al., 2019). The XRD pattern of fresh WO_3/SiC has reflections characteristic of SiC, WO_3 (JCPDS No.01-077-1317) and SiO_2 (JCPDS No.01-087-2096) (Pourasad et al., 2016; Vairojanakit and Sinchai, 2019). The latter phase was also identified in the XRD patterns of 5NaW/SiC and 5NaW-3Mn/SiC. This means that WO_3 and Na_2WO_4 can partially

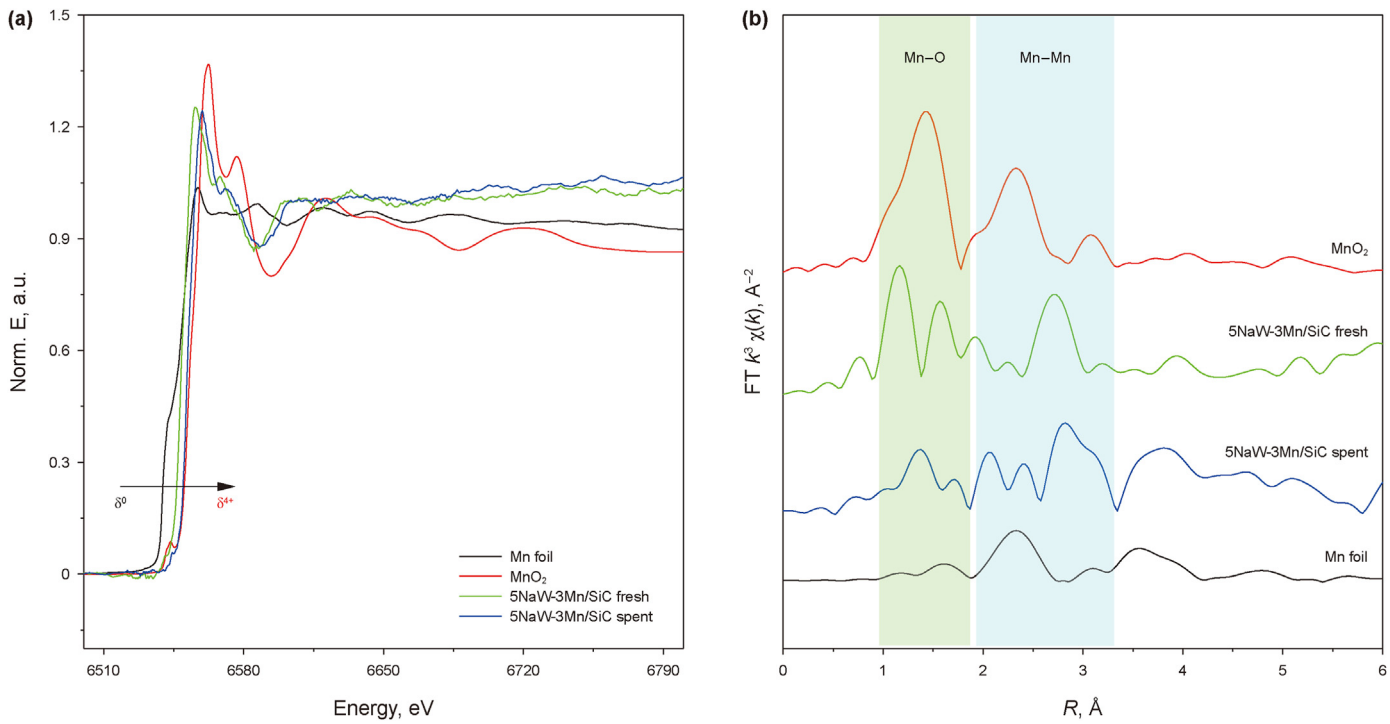

Fig. 9. **(a)** Experimental XANES spectra at the Cu K edge over 5NaW-3Mn/SiC fresh and spent with water, **(b)** FT k^3-weighted $\chi(k)$ function of the EXAFS spectra over 5NaW-3Mn/SiC fresh and spent with steam.

Table 2
The surface atomic composition of fresh and spent (after OCM with co-fed steam) catalysts of 5NaW-3Mn/SiC.

	Si 2p	C 1s	Na 1s	W 4f	Mn 2p	O 1s
Fresh catalyst atomic, %	21.94	35.99	0.99	0.29	0.48	21.94
Spent catalyst atomic, %	24.08	23.28	1.74	0.51	0.78	49.62

Table 3
The total atomic composition of fresh and spent catalysts of 5NaW-3Mn/SiC.

	Si	Na	W	Mn
Fresh catalyst atomic, %	39.7	0.21	1.33	2.09
Spent catalyst atomic, %	40.1	0.22	1.48	2.53

oxidize SiC to SiO_2. According to a previous study (Sourav et al., 2021), WO_3 and Na_2WO_4 can store oxygen, which may be responsible for this oxidation reaction.

In addition to SiC and SiO_2, the Na_2WO_4 phase (Na_2WO_4, JCPDS No.00-020-1163) is present in the 5NaW/SiC and 5NaW-3Mn/SiC catalysts. However, in contrast to the former catalyst, no reflections characteristic of MnO_2 could be identified in the XRD pattern of the 5NaW-3Mn/SiC catalyst, which also contains crystalline $Mn_7O_8(SiO_4)$ characterized by the reflection at 2θ of 33.0° (JCPDS No.01-089-5662) (Aydin et al., 2021).

After OCM tests with co-fed steam, the diffraction peaks of the MnO_x-related phases in spent 3Mn/SiC disappeared (Fig. 8(b)) due to their redispersion. This finding is also valid for other spent Mn-containing catalysts. In addition, the intensity of the reflections characteristic of SiC decreased, while those of SiO_2 increased in spent WO_3/SiC, 5NaW/SiC and 5NaW-3Mn/SiC after OCM with co-fed steam.

3.3. Chemical properties of catalysts

The local atomic and electronic structure of Mn in fresh and spent (after OCM with co-fed steam) 5NaW-3Mn/SiC was characterized by X-ray absorption fine structure spectroscopy (XAFS). Based on the X-ray absorption near edge structure (XANES) spectra (Fig. 9(a)), the oxidation state of Mn should be between MnO_2 and metallic Mn^0 in the spent catalyst as compared to its fresh counterpart. The fresh and spent catalysts also differ in the local coordination on manganese. According to the EXAFS spectra (Fig. 9(b)), the first shell scattering at 1.4 Å and 1.6 Å corresponds to O neighbors in the fresh and spent catalysts. The corresponding distances of the second shell scattering (Mn-Mn) are 2 Å to 3 Å.

The surface composition of fresh and spent (after OCM with co-fed steam) 5NaW-3Mn/SiC was analyzed by XPS (Table 2). The content of Si, Na, W and Mn slightly increased after performing the OCM reaction with steam, while the content of C and O decreased and increased obviously, respectively. This is due to the oxidation of SiC to SiO_2 as also seen by XRD (Fig. 8(e)). From the ICP-OES analysis (Table 3), the total atomic composition of Si, Na, W and Mn keep did not change after the OCM reaction.

The signals at about 534.8 and 535.0 eV in the XPS spectra of O 1s of fresh and spent catalysts, respectively (Fig. 10(b)) can be attributed to Si–O interactions, which turns out that SiC can react with dissolved oxygen with the help of Na_2WO_4 to convert to SiO_2 (Sinev et al., 2019). The signals at about 532.9 and 532.7 eV can be ascribed to Mn–O bond and Na–O–W bonds, respectively (Torshizi

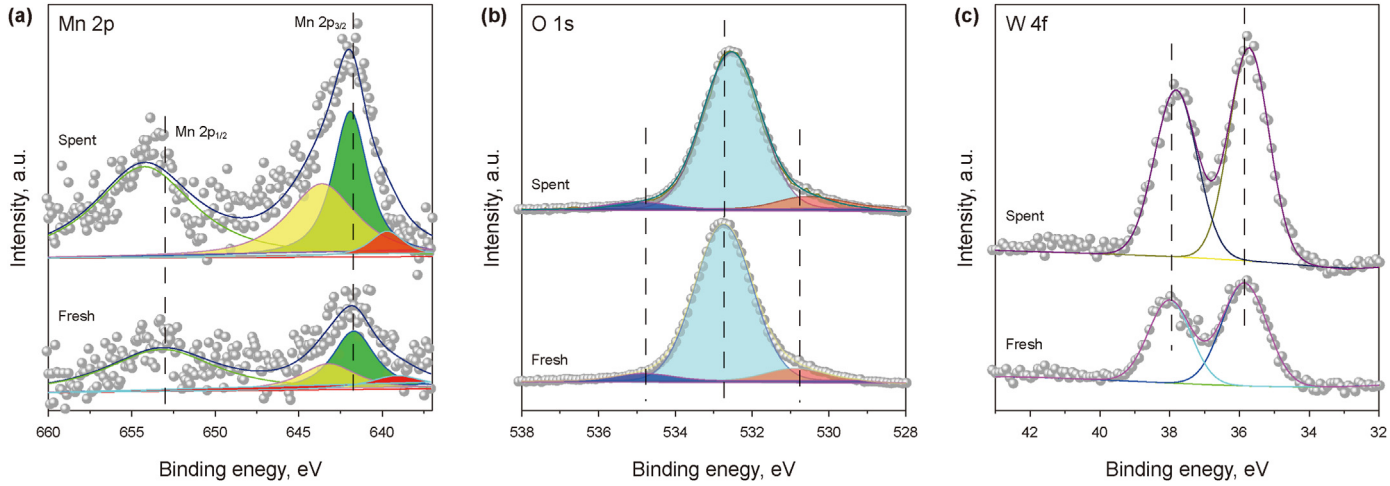

Fig. 10. The Mn 2p **(a)**, O 1s **(b)** and W 4f **(c)** peaks of XPS survey spectra over 5NaW-3Mn/SiC fresh and spent with steam.

et al., 2024; Vovk et al., 2024). The XPS survey spectra of O 1s and W 4f signals shifted to a lower energy after OCM, while the signals characteristic of Mn^{2+} (639.7 eV), Mn^{3+} (641.7 eV) and Mn^{4+} (643.2 eV) (Fig. 10) (Fang et al., 2023) shifted to a higher energy. This result suggests that Mn provided some electron density to O and W probably due to an increased dispersion of MnO_x species as evidenced by STEM mapping (Fig. 5(l)). It may be one of the reasons to increase the selectivity to C_{2+}-hydrocarbons.

To check if the above-discussed structural changes are relevant to redox properties of 5NaW-3Mn/SiC catalyst, we performed temperature-programmed reduction tests with H_2 (H_2-TPR) using its fresh and spent (after OCM tests without or with steam) samples, as well as fresh 3Mn/SiC and 5NaW/SiC for comparative purposes. The latter catalysts did not consume H_2 in the total temperature range between room temperature and 900 °C. Only one peak of H_2 consumption with the maximal rate at 513 °C is seen in the H_2-TPR profile of 3Mn/SiC (Fig. 11). It can be assigned to the reduction of Mn_2O_3 to Mn_3O_4 (Jiang et al., 2016; Shahri and Alavi, 2009). Two H_2 hydrogen consumption peaks with the maxima at 660 and 860 °C are present in the H_2-TPR profiles of fresh, and spent 5NaW-3Mn/SiC. The low-temperature peak is due to the reduction of Mn_2O_3 to Mn_3O_4, and the high-temperature peak should belong to the reduction of Mn_3O_4 to MnO (Jiang et al., 2016; Sun et al., 2022; Zhang et al., 2017). The coexistence of Na_2WO_4 and MnO_x changes the oxidation-reduction ability of the 5NaW-3Mn/SiC catalyst. It was also found that the low-temperature peak of H_2 consumption over fresh 5NaW-3Mn/SiC moved to lower temperatures after OCM test without steam. In contrast, it moved to higher temperatures after OCM test with steam. These results suggest that steam-induced catalyst restructuring can also change the oxidation-reduction ability of the 5NaW-3Mn/SiC catalyst.

3.4. Selectivity-conversion relationships and reaction pathways of catalysts with and without steam

Further insights into the role of steam in product formation in the course of the OCM reaction over the 5NaW-3Mn/SiC catalyst were derived from analyzing the selectivity-conversion relationships for C_2H_6, C_2H_4, CO and CO_2. These relationships were obtained using the results of catalytic tests performed at 800 °C but different contact times. In the absence of steam, the selectivity values of CO, CO_2, and C_2H_6 extrapolated to a zero conversion of methane are not zero (Fig. 12). Thus, these products are formed directly from CH_4. The extrapolated C_2H_4 selectivity is zero, i.e., this product should be formed from C_2H_6 as can be concluded from the fact that the selectivity to C_2H_4 increases, while the selectivity to C_2H_6 decreases with increasing methane conversion. The latter decrease can also be partially due to the oxidation of ethane to carbon dioxide, because the selectivity to the latter product increases with increasing CH_4 conversion. However, the main pathway leading to CO_2 is the oxidation of CO. Although this general scheme of product formation does not change in the presence of steam, this feed component inhibits the direct oxidation of CH_4 to CO and CO_2. This conclusion was made based on the fact that the selectivity values of CO and CO_2 extrapolated to a zero CH_4 conversion are lower in the presence of steam.

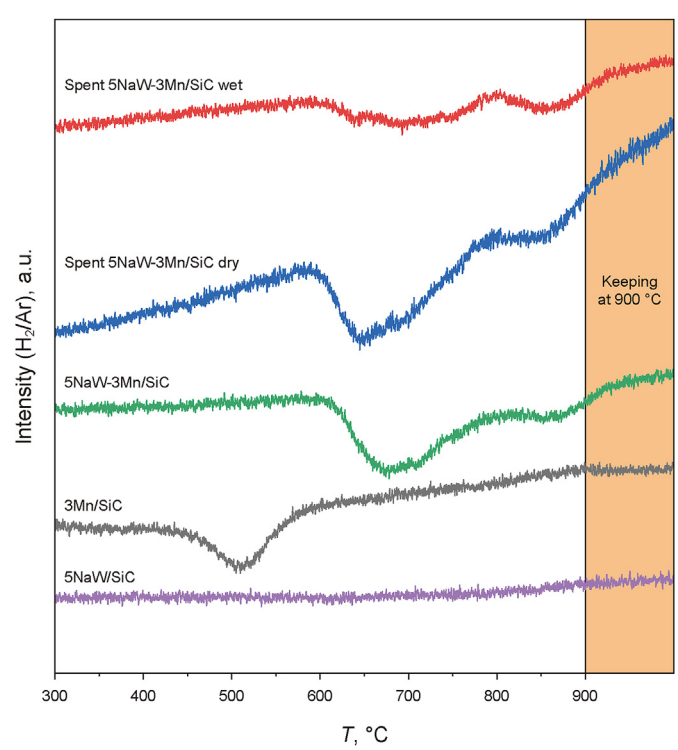

Fig. 11. H_2-TPR profiles of 3Mn/SiC, 5NaW/SiC, fresh, spent 5NaW-3Mn/SiC with and without steam.

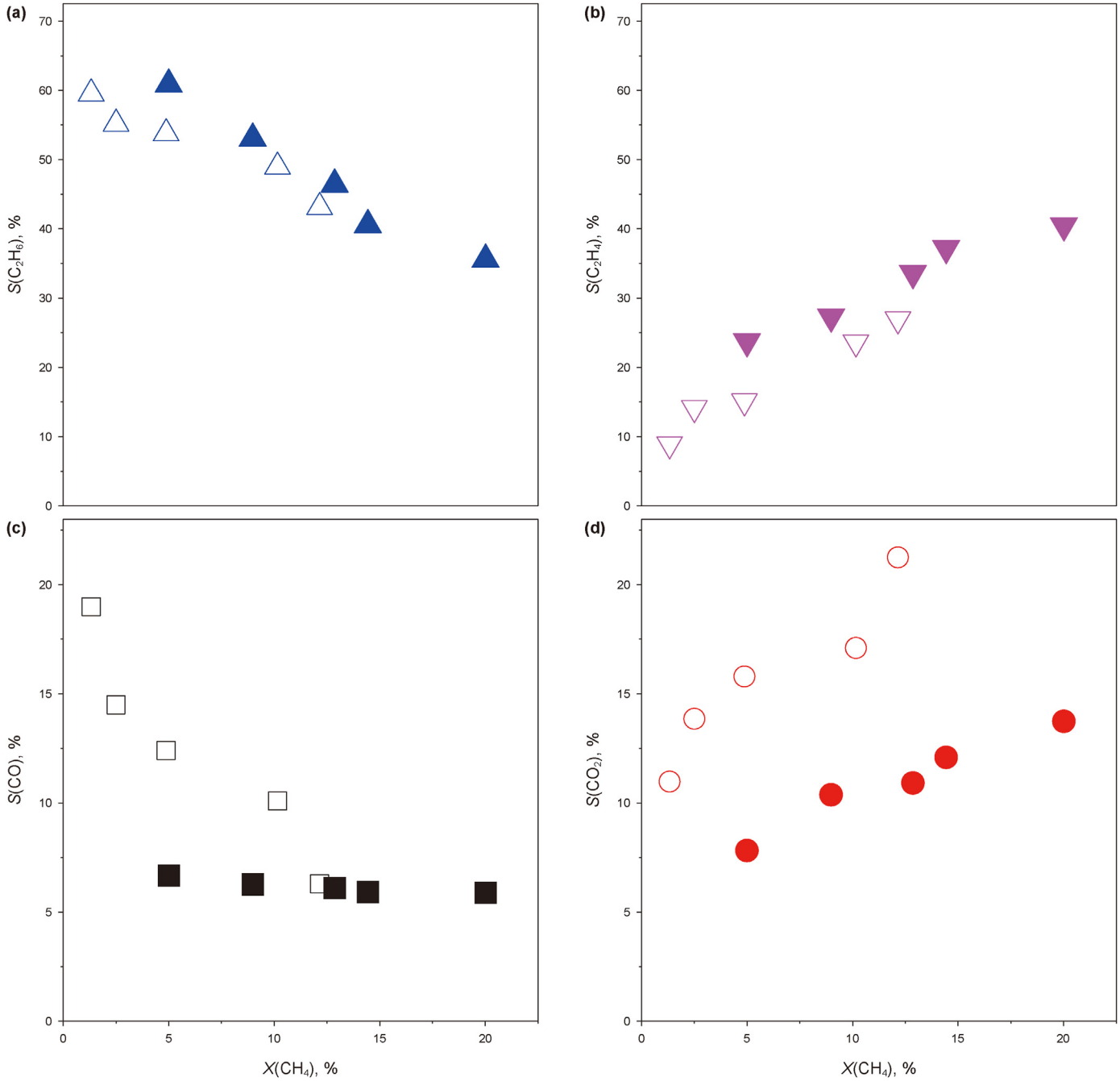

Fig. 12. The selectivity to **(a)** C_2H_6, **(b)** C_2H_4, **(c)** CO and **(d)** CO_2 as a function of CH_4 conversion without (open symbols) and with 30 vol% (filled symbols) steam at 800 °C over the catalyst of 5NaW-3Mn/SiC.

From the analysis of relevant literature and our data, especially the selectivity-conversion relationships in Fig. 12, an overall scheme of the formation of C_2H_4, C_2H_6, CO and CO_2 in the course of the OCM reaction was obtained (Scheme 1). C_2H_6, CO and CO_2 are directly formed from CH_4 both with and without steam. The latter feed component enhances the formation of C_2H_6 and decrease the direct oxidation of methane to CO and CO_2. The positive effect of steam on C_2H_6 formation can be partially assigned to the redispersion of MnO_x species.

4. Conclusion

In summary, this work reports a positive effect of steam on the selectivity to C_2-hydrocarbons in the OCM reaction over 5NaW-3Mn/SiC. In contrast to the NaWMn/SiO_2 system, for which the steam effect has been originally discovered, this effect is also pronounced above 800 °C for the 5NaW-3Mn/SiC catalyst developed in this study. The difference can be due to interactions of SiC, MnO_x and Na_2WO_4 with each other resulting in heterojunctions and

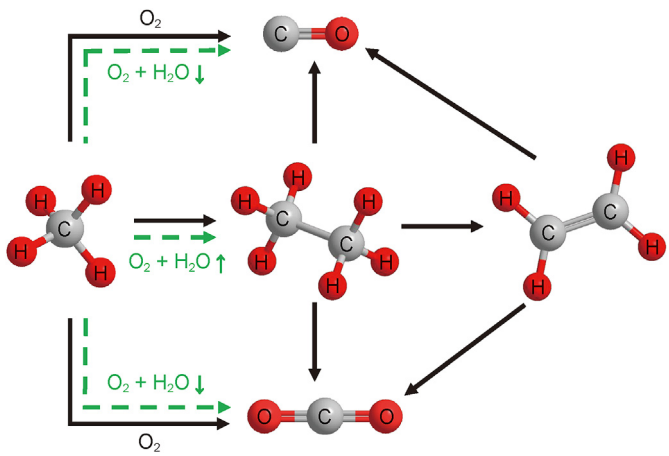

Scheme 1. The reaction pathways in OCM reaction over 5NaW-3Mn/SiC catalyst with and without steam.

accordingly modifications of electronic properties as indirectly supported by the formation of Moiré superlattices. Advanced characterization by STEM, XPS and XAS shows that steam increases the dispersion of MnO_x and reduces the surface area of the catalyst. These changes appear to be important for increasing the selectivity to C_2-hydrocarbons. Although steam accelerates the rates of CO, CO_2, C_2H_4 and C_2H_6 formation, the overall scheme of the formation of these products is not changed. As the highest enhancement was determined for the latter two products, the contribution of the direct oxidation of methane to carbon oxides decreases by steam.

CRediT authorship contribution statement

Juan Chen: Writing – original draft. **Jian-Shu Li:** Writing – original draft. **Anna Zanina:** Investigation, Data curation. **Wen Jiang:** Investigation, Data curation. **Yu-Ming Li:** Writing – review & editing. **Gui-Yuan Jiang:** Writing – review & editing. **Evgenii V. Kondratenko:** Writing – review & editing.

Declaration of interests

The authors declare that they have no known competing financial interests or personal relationships that could have appeared to influence the work reported in this paper.

Acknowledgement

This work is supported by the National Key Research and Development Program (Nos. 2020YFA0210903), the National Natural Science Foundation of China (Grant Nos. 22225807, 21961132026, 22021004) and DFG within joint Sino-German project (KO 2261/11-1).

References

Abbas, G., Li, Y., Wang, H., et al., 2020. Recent advances in twisted structures of flatland materials and crafting moiré superlattices. Adv. Funct. Mater. 30 (36), 2000878. https://doi.org/10.1002/adfm.202000878.

Ahn, S.J., Moon, P., Kim, T.-H., et al., 2018. Dirac electrons in a dodecagonal graphene quasicrystal. Science 361 (6404), 782–786. https://www.science.org/doi/full/10.1126/science.aar8412.

Alzahrani, S.M.S., Lobban, L.L., 1995. Effects of steam and liquid water treatment on the oxidative coupling of methane over a Li/MgO catalyst. Ind. Eng. Chem. Res. 34 (4), 1060–1073. https://doi.org/10.1021/ie00043a007.

Aydin, Z., Kondratenko, V.A., Lund, H., et al., 2020. Revisiting activity- and selectivity-enhancing effects of water in the oxidative coupling of methane over MnO_x-Na_2WO_4/SiO_2 and proving for other materials. ACS Catal. 10 (15), 8751–8764. https://doi.org/10.1021/acscatal.0c01493.

Aydin, Z., Zanina, A., Kondratenko, V.A., et al., 2021. Elucidating the effects of individual components in K_xMnO_y/SiO_2 and water on selectivity enhancement in the oxidative coupling of methane. Catal. Sci. Technol. 11 (17), 5827–5838. https://doi.org/10.1039/D1CY01081F.

Aydin, Z., Zanina, A., Kondratenko, V.A., et al., 2022. Effects of N_2O and water on activity and selectivity in the oxidative coupling of methane over Mn-Na_2WO_4/SiO_2: role of oxygen species. ACS Catal. 12 (2), 1298–1309. https://doi.org/10.1021/acscatal.1c04915.

Bostwick, A., Ohta, T., Seyller, T., et al., 2007. Quasiparticle dynamics in graphene. Nat. Phys. 3 (1), 36–40. https://doi.org/10.1038/nphys477.

Chin, Y.-H., Buda, C., Neurock, M., et al., 2011. Reactivity of chemisorbed oxygen atoms and their catalytic consequences during CH_4–O_2 catalysis on supported Pt clusters. J. Am. Chem. Soc. 133 (40), 15958–15978. https://doi.org/10.1021/ja202411v.

Deng, B., Wang, B., Li, N., et al., 2020. Interlayer decoupling in 30° twisted bilayer graphene quasicrystal. ACS Nano 14 (2), 1656–1664. https://doi.org/10.1021/acsnano.9b07091.

Dooley, K.M., Chen, S.Y., Ross, J.R.H., 1994. Stable nickel-containing catalysts for the oxidative coupling of methane. J. Catal. 145 (2), 402–408. https://doi.org/10.1006/jcat.1994.1050.

Ercolino, G., Stelmachowski, P., Specchia, S., 2017. Catalytic performance of Pd/Co_3O_4 on SiC and ZrO_2 open cell foams for process intensification of methane combustion in lean conditions. Ind. Eng. Chem. Res. 56 (23), 6625–6636. https://doi.org/10.1021/acs.iecr.7b01087.

Fang, D.C., Zheng, J.Y., Han, C.B., et al., 2023. Electro-injection-enhanced catalytic formaldehyde degradation based on conductive MnOx cellulose aerogels at room temperature. Appl. Catal., B. 334, 122837. https://doi.org/10.1016/j.apcatb.2023.122837.

Fang, X., Li, S., Lin, J., et al., 1992a. Oxidative coupling of methane on W-Mn catalysts. J. Mol. Catal. 6 (6), 427–433. https://doi.org/10.16084/j.cnki.issn1001-3555.1992.06.004.

Fang, X., Li, S., Lin, J., et al., 1992b. Preparation and characterization of W-Mn catalyst for oxidative coupling of methane. J. Mol. Catal. 6 (4), 255–262. https://doi.org/10.16084/j.cnki.issn1001-3555.1992.04.003 (in Chinese).

Fleischer, V., Simon, U., Parishan, S., et al., 2018. Investigation of the role of the $Na_2WO_4/Mn/SiO_2$ catalyst composition in the oxidative coupling of methane by chemical looping experiments. J. Catal. 360, 102–117. https://doi.org/10.1016/j.jcat.2018.01.022.

He, F., Zhou, Y., Ye, Z., et al., 2021. Moiré patterns in 2D materials: a review. ACS Nano 15 (4), 5944–5958. https://doi.org/10.1021/acsnano.0c10435.

Holmen, A., 2009. Direct conversion of methane to fuels and chemicals. Catal. Today 142 (1), 2–8. https://doi.org/10.1016/j.cattod.2009.01.004.

Jiang, H., Wang, C., Wang, H., et al., 2016. Synthesis of highly efficient MnOx catalyst for low-temperature NH_3-SCR prepared from Mn-MOF-74 template. Mater. Lett. 168, 17–19. https://doi.org/10.1016/j.matlet.2015.12.150.

Keller, G.E., Bhasin, M.M., 1982. Synthesis of ethylene via oxidative coupling of methane: I. Determination of active catalysts. J. Catal. 73 (1), 9–19. https://doi.org/10.1016/0021-9517(82)90075-6.

Kondratenko, E.V., Peppel, T., Seeburg, D., et al., 2017. Methane conversion into different hydrocarbons or oxygenates: current status and future perspectives in catalyst development and reactor operation. Catal. Sci. Technol. 7 (2), 366–381. https://doi.org/10.1039/C6CY01879C.

Le, T.A., Kang, J.K., Park, E.D., 2018. CO and CO_2 methanation over Ni/SiC and Ni/SiO_2 catalysts. Top. Catal. 61 (15), 1537–1544. https://doi.org/10.1007/s11244-018-0965-7.

Li, D., Baslyman, W.S., Sarathy, S.M., et al., 2020. Impact of OH radical generator involvement in the gas-phase radical reaction network on the oxidative coupling of methane—a simulation study. Energy Tech. 8 (8), 1900563. https://doi.org/10.1002/ente.201900563.

Li, D., Yoshida, S., Siritanaratkul, B., et al., 2021. Transient potassium peroxide species in highly selective oxidative coupling of methane over an unmolten K_2WO_4/SiO_2 catalyst revealed by in situ characterization. ACS Catal. 11 (22), 14237–14248. https://doi.org/10.1021/acscatal.1c04206.

Li, J., Chen, J., Zanina, A., et al., 2023. Fundamentals of enhanced oxygen releasability of Mn-Na_2WO_4/SiO_2 through cofed water for efficient oxidative coupling of methane in a chemical looping mode. J. Catal. 428, 115176. https://doi.org/10.1016/j.jcat.2023.115176.

Li, S., 2001. Oxidative coupling of methane over W-Mn/SiO_2 catalyst. Chin. J. Chem. 19 (1), 16–21. https://doi.org/10.1002/cjoc.20010190104.

Li, X., Tomishige, K., Fujimoto, K., 1996. Oxidative coupling of methane by water as the oxidant on perovskite oxide catalysts. Catal. Lett. 36 (1), 21–24. https://doi.org/10.1007/BF00807200.

Li, X., Xie, J., Rao, H., et al., 2020. Platinum- and CuOx-decorated TiO_2 photocatalyst for oxidative coupling of methane to C_2 hydrocarbons in a flow reactor. Angew. Chem., Int. Ed. 59 (44), 19702–19707. https://doi.org/10.1002/anie.202007557.

Li, Y., Wan, Q., Xu, N., 2023. Recent advances in moiré superlattice systems by angle-resolved photoemission spectroscopy. Adv. Mater., 2305175 https://doi.org/10.1002/adma.202305175.

Liang, Y., Li, Z., Nourdine, M., et al., 2014. Methane coupling reaction in an oxy-steam stream through an OH radical pathway by using supported alkali metal catalysts. ChemCatChem. 6 (5), 1245–1251. https://doi.org/10.1002/cctc.201400018.

Liao, M., Wang, C., Bu, E., et al., 2019. Efficient hydrogen production from partial oxidation of propane over SiC doped Ni/Al_2O_3 catalyst. Energy Proc. 158,

1772–1779. https://doi.org/10.1016/j.egypro.2019.01.419.
Liu, H., Yang, D., Gao, R., et al., 2008. A novel Na_2WO_4–Mn/SiC monolithic foam catalyst with improved thermal properties for the oxidative coupling of methane. Catal. Commun. 9 (6), 1302–1306. https://doi.org/10.1016/j.catcom.2007.11.022.
Liu, J., Yue, J., Lv, M., et al., 2022. From fundamentals to chemical engineering on oxidative coupling of methane for ethylene production: a review. Carbon Resour. Convers. 5 (1), 1–14. https://doi.org/10.1016/j.crcon.2021.11.001.
Liu, Y., Zeng, C., Yu, J., et al., 2021. Moiré superlattices and related moiré excitons in twisted van der Waals heterostructures. Chem. Soc. Rev. 50 (11), 6401–6422. https://doi.org/10.1039/D0CS01002B.
Lolupiman, K., Wangyao, P., Qin, J., 2019. Electrodeposition of Zn/TiO_2 composite coatings for anode materials of Zinc ion battery. J. Min. Met. Mater. 29 (4), 120–126. https://doi.org/10.55713/jmmm.v29i4.652.
Lomonosov, V., Gordienko, Y., Sinev, M., 2013. Effect of water on methane and ethane oxidation in the conditions of oxidative coupling of methane over model catalysts. Top. Catal. 56 (18), 1858–1866. https://doi.org/10.1007/s11244-013-0122-2.
Matsumoto, T., Saito, M., Ishikawa, S., et al., 2020. High catalytic activity of crystalline lithium calcium silicate for oxidative coupling of methane originated from crystallographic joint effects of multiple cations. ChemCatChem. 12 (7), 1968–1972. https://doi.org/10.1002/cctc.201902241.
Novoselov, K.S., Geim, A.K., Morozov, S.V., et al., 2005. Two-dimensional gas of massless Dirac fermions in graphene. Nature 438 (7065), 197–200. https://doi.org/10.1038/nature04233.
Novoselov, K.S., Geim, A.K., Morozov, S.V., et al., 2004. Electric field effect in atomically thin carbon films. Science 306 (5696), 666–669. https://doi.org/10.1126/science.1102896.
Pak, S., Qiu, P., Lunsford, J.H., 1998. Elementary reactions in the oxidative coupling of methane over Mn/Na_2WO_4/SiO_2 and Mn/Na_2WO_4/MgO catalysts. J. Catal. 179 (1), 222–230. https://doi.org/10.1006/jcat.1998.2228.
Pereira, P., Lee, S.H., Somorjai, G.A., et al., 1990. The conversion of methane to ethylene and ethane with near total selectivity by low temperature (< 610 °C) oxydehydrogenation over a calcium-nickel-potassium oxide catalyst. Catal. Lett. 6 (3–6), 255–262. https://doi.org/10.1007/BF00763991.
Pourasad, J., Ehsani, N., Khalifesoltani, S.A., 2016. Preparation and characterization of SiO_2 thin film and SiC nanofibers to improve of graphite oxidation resistance. J. Eur. Ceram. Soc. 36 (16), 3947–3956. https://doi.org/10.1016/j.jeurceramsoc.2016.06.046.
Schwach, P., Pan, X., Bao, X., 2017. Direct conversion of methane to value-added chemicals over heterogeneous catalysts: challenges and prospects. Chem. Rev. 117 (13), 8497–8520. https://doi.org/10.1021/acs.chemrev.6b00715.
Shahri, S.M.K., Alavi, S.M., 2009. Kinetic studies of the oxidative coupling of methane over the Mn/Na_2WO_4/SiO_2 catalyst. J. Nat. Gas Chem. 18 (1), 25–34. https://doi.org/10.1016/S1003-9953(08)60079-1.
Shimizu, T., Kitayama, Y., Kodama, T., 2001. Thermochemical conversion of CH_4 to C_2-hydrocarbons and H_2 over SnO_2/Fe_3O_4/SiO_2 in Methane–Water Co-feed system. Energy & Fuels 15 (2), 463–469. https://doi.org/10.1021/ef000200w.
Sinev, M., Ponomareva, E., Sinev, I., et al., 2019. Oxygen pathways in oxidative coupling of methane and related processes. Case study: NaWMn/SiO_2 catalyst. Catal. Today 333, 36–46. https://doi.org/10.1016/j.cattod.2018.06.028.
Sourav, S., Wang, Y., Kiani, D., et al., 2021. New mechanistic and reaction pathway insights for oxidative coupling of methane (OCM) over supported Na_2WO_4/SiO_2 catalysts. Angew. Chem., Int. Ed. 60 (39), 21502–21511. https://doi.org/10.1002/anie.202108201.
Sun, W., Zhao, G., Gao, Y., et al., 2022. An oxygen carrier catalyst toward efficient chemical looping-oxidative coupling of methane. Appl. Catal. B Environ. 304, 120948. https://doi.org/10.1016/j.apcatb.2021.120948.
Takanabe, K., Iglesia, E., 2009. Mechanistic aspects and reaction pathways for oxidative coupling of methane on Mn/Na_2WO_4/SiO_2 catalysts. J. Phys. Chem. C. 113 (23), 10131–10145. https://doi.org/10.1021/jp9001302.
Takanabe, K., Iglesia, E., 2008. Rate and selectivity enhancements mediated by OH radicals in the oxidative coupling of methane catalyzed by Mn/Na_2WO_4/SiO_2. Angew. Chem., Int. Ed. 47 (40), 7689–7693. https://doi.org/10.1002/anie.200802608.
Tang, P., Zhu, Q., Wu, Z., et al., 2014. Methane activation: the past and future. Environ. Eng. Sci. 7 (8), 2580–2591. https://doi.org/10.1039/C4EE00604F.
Torshizi, H.O., Nakhaei Pour, A., Salimi, A., et al., 2024. Support effect of Mn/Na_2WO_4-based catalysts in oxidative coupling of methane. J. Chem. Technol. Biotechnol. 99 (2), 405–414. https://doi.org/10.1002/jctb.7542.
Vairojanakit, C., Sinchai, S., 2019. Influence of mechanical activation on the phase formation in the synthesis of cordierite from talc and andalusite. Key Eng. Mater. 798, 235–241. https://doi.org/10.4028/www.scientific.net/KEM.798.235.
Vovk, E.I., Wang, D., Qiu, Z., et al., 2024. In situ structure study of a TiO_2 doped MnO_X-Na_2WO_4/SiO_2 catalyst under Na_2WO_4 melting conditions. Top. Catal. https://doi.org/10.1007/s11244-024-01946-4.
Wang, H., Schmack, R., Paul, B., et al., 2017. Porous silicon carbide as a support for Mn/Na/W/SiC catalyst in the oxidative coupling of methane. Appl. Catal. A. 537, 33–39. https://doi.org/10.1016/j.apcata.2017.02.018.
Wang, H., Schmack, R., Sokolov, S., et al., 2022. Oxide-supported carbonates reveal a unique descriptor for catalytic performance in the oxidative coupling of methane (OCM). ACS Catal. 12 (15), 9325–9338. https://doi.org/10.1021/acscatal.1c05177.
Wang, Y., Hu, P., Yang, J., et al., 2021. C-H bond activation in light alkanes: a theoretical perspective. Chem. Soc. Rev. 50 (7), 4299–4358. https://doi.org/10.1039/D0CS01262A.
Weng, W., Chen, M., Wan, H., et al., 1998. High-temperature in situ FTIR spectroscopy study of LaOF and BaF_2/LaOF catalysts for methane oxidative coupling. Catal. Lett. 53 (1), 43–50. https://doi.org/10.1023/A:1019037301983.
Werny, M.J., Wang, Y., Girgsdies, F., et al., 2020. Fluctuating storage of the active phase in a Mn-Na_2WO_4/SiO_2 catalyst for the oxidative coupling of methane. Angew. Chem., Int. Ed. 59 (35), 14921–14926. https://doi.org/10.1002/anie.202004778.
Xu, J., Xi, R., Gong, Y., et al., 2022. Constructing $Y_2B_2O_7$ (B = Ti, Sn, Zr, Ce) compounds to disclose the effect of surface acidity–basicity on product selectivity for oxidative coupling of methane (OCM). Inorg. Chem. 61 (29), 11419–11431. https://doi.org/10.1021/acs.inorgchem.2c01754.
Xu, L., Zanina, A., Wu, K., et al., 2023. Breaking the dilemma of low selectivity in the oxidative coupling of methane over Mn-Na_2WO_4/SiO_2 at low temperatures. Chem. Eng. J. 473, 145372. https://doi.org/10.1016/j.cej.2023.145372.
Xu, M., Guo, L., Fu, Y., 2021. Effect of pyrocarbon texture on the mechanical and oxidative erosion property of SiC coating for protecting carbon/carbon composites. Ceram. Int. 47 (23), 32657–32665. https://doi.org/10.1016/j.ceramint.2021.08.162.
Yan, C., Ma, D.L., Qiao, J.B., et al., 2019. Scanning tunneling microscopy study of the quasicrystalline 30° twisted bilayer graphene. 2D Mater. 6 (4), 045041. https://doi.org/10.1088/2053-1583/ab3b16.
Yang, J., Wang, L., Ma, Z., et al., 2019. In situ synthesis of Mn_3O_4 on Ni foam/graphene substrate as a newly self-supported electrode for high supercapacitive performance. J. Colloid Interface Sci. 534, 665–671. https://doi.org/10.1016/j.jcis.2018.09.077.
Yao, W., Wang, E., Bao, C., et al., 2018. Quasicrystalline 30° twisted bilayer graphene as an incommensurate superlattice with strong interlayer coupling. P. Natl. Acad. Sci. Usa. 115 (27), 6928–6933. https://doi.org/10.1073/pnas.1720865115.
Zanina, A., Kondratenko, V.A., Lund, H., et al., 2023. Performance-defining factors of (MnO_x)-M_2WO_4/SiO_2 (M = Na, K, Rb, or Cs) catalysts in oxidative coupling of methane. J. Catal. 419, 68–79. https://doi.org/10.1016/j.jcat.2023.02.004.
Zanina, A., Kondratenko, V.A., Lund, H., et al., 2022. The role of adsorbed and lattice oxygen species in product formation in the oxidative coupling of methane over M_2WO_4/SiO_2 (M = Na, K, Rb, Cs). ACS Catal. 12 (24), 15361–15372. https://doi.org/10.1021/acscatal.2c04916.
Zanina, A., Kondratenko, V.A., Makhmutov, D., et al., 2024. Elucidating the role of oxygen species in oxidative coupling of methane over supported MnO_x–Na_2WO_4 containing catalysts. ChemCatChem 16 (2), e202300885. https://doi.org/10.1002/cctc.202300885.
Zhang, X., Li, H., Hou, F., et al., 2017. Synthesis of highly efficient Mn_2O_3 catalysts for CO oxidation derived from Mn-MIL-100. Appl. Surf. Sci. 411, 27–33. https://doi.org/10.1016/j.apsusc.2017.03.179.